Wakefield induced Losses in the Manual Valves of the TESLA Cryomodule

M. Dohlus, H.-P. Wedekind, K. Zapfe

Deutsches Elektronen Synchrotron

Notkestr. 85, D-22603 Hamburg, Germany

Abstract

The beam pipe of the TESLA cryomodule is closed off by manual valves on both sides of the string of 12 cavities. Compared to the manual valves with spring type rf-shield which are presently used in the linac of the TESLA Test Facility a simplified version will be needed by cost reasons for the TESLA linear collider. Therefore wakefield induced losses for two simplified valve geometries have been studied in detail. Three types of losses are distinguished: transient and resonant losses due to wake fields induced by the valves themselves and losses due to wakes induced in the cavities. The calculations have been done for two different operation modes - linac operation and FEL operation. In addition the transverse kick has been calculated and compared with the strongest kick from a nine cell cavity. The results show, that the losses from a valve with simplified rf-shield are acceptable.

1. Introduction

One of the major objectives for the beam vacuum system of that part of the TESLA linear collider containing the superconducting cavities is to preserve the cleanliness of the cavities' surfaces and thus the operation at high gradients and high Q. Contamination by any sort of dust or condensation of gases during assembly, testing and operation has to be absolutely minimized. Therefore the string of 12 cavities and the beam pipe of the superconducting quadrupole are evacuated and closed off by manual all metal valves at both ends of the string in the clean room after assembly.

For the cryogenic system power losses induced by wakefields in the manual valves are of major concern. The manual valves presently used in the linac of the TESLA Test Facility are all metal valves with spring type rf-shielding, so power losses by wake fields should be small. However this solution is rather expensive compared to standard valves. Additionally there is some concern of the production of metallic dust particles by the rf-shields. Thus simplifications of the manual valves are under study for the TESLA linear collider.

In the following wakefield induced power losses and kicks for two simplified versions of the manual valves are studied in detail.

2. Calculations of Electrical Losses and Kicks

The wakefields, which cause power losses in the manual valves, can be separated into wakefields, which are induced by the valves (see section 2.1) and wakefields due to other discontinuities in the LINAC (see section 2.2).

The losses of the valve wakefields can be split into high frequency components that can propagate through the beam pipe and trapped modes, which may cause resonant losses. The high frequency components are estimated by calculating the "**single bunch losses**", where it is assumed that the total energy lost during the passage of a single bunch is dissipated until the next bunch enters the valve (see section 2.1.1). The "**resonant losses**" take into account all modes, which are below the lowest dipole cutoff frequency of the beam pipe and are therefore trapped in the manual valve (see section 2.1.2). While the single bunch losses are a pure geometrical property, the resonant losses depend on the surface conductivity of the valve.

The transverse asymmetry of the valves causes a field asymmetry and thus a deflection of the bunches. The transverse kick parameters of all modes below the lowest dipole cutoff frequency are compared with the kick parameters of to the strongest dipole modes of a TESLA 9-cell cavity for an offset of 0.5mm (see section 2.1.3).

The numerical results for two types of operational conditions (see section 2.1.4) and two valve geometries are listed in the section 2.1.5 and 2.1.6.

2.1. Fields Induced by the Manual Valves

2.1.1. Single Bunch Losses

The single bunch losses $P^{(\mathrm{single})}$ can be calculated from the longitudinal electrical field $E_z^{(\sigma)}(z,t)$ that is induced by a bunch of length σ as follows:

$$w_{\parallel}^{(\sigma)}(s) = \frac{1}{q}\int_{-\infty}^{\infty} E_z^{(\sigma)}(z-s, z/c_0)dz\,,$$

$$k_{\parallel}^{(\sigma)} = -\int_{-\infty}^{\infty} w_z^{(\sigma)}(s)\frac{g(s/\sigma)}{\sigma}ds\,,$$

$$W = q^2 k_{\parallel}^{(\sigma)}(\sigma)\,,$$

$$P^{(\mathrm{single})} = \frac{W}{T_{\mathrm{bunch}}} T_{\mathrm{pulse}} f_{\mathrm{rep}}\,, \qquad (1)$$

with c_0 the velocity of light, q the bunch charge, $w_{\parallel}^{(\sigma)}(s)$ the normalized longitudinal wake function, s the distance from the bunch center to the observation particle, $k_{\parallel}^{(\sigma)}$ the longitudinal loss parameter, $g(s)$ the Gaussian normal distribution, W the energy loss of one bunch, T_{bunch} the bunch spacing, T_{pulse} the length of rf pulse (flat top) and f_{rep} the repetition rate. In most of the cases described in sections 2.1.5 and 2.1.6 the required field calculations could be done directly [1]. Only for gaps of length l_{gap} with very extreme ratios of l_{gap}/σ the loss parameter is estimated using the diffraction model [2]:

$$k_{\parallel}^{(\sigma,\text{gap})} = \frac{\Gamma(1/4)}{4\pi^2\varepsilon_0 r}\sqrt{\frac{l_{gap}}{\pi\sigma}}, \tag{2}$$

with r the beam pipe radius.

2.1.2. Resonant Losses

The contribution of resonant modes to the longitudinal wake function is

$$w_{\parallel}(s) = \text{Re}\left\{\sum_{\nu} 2k_{\parallel}^{(\nu)} \exp\left(\frac{p^{(\nu)}}{c_0}s\right)\right\} \cdot \begin{cases} 0 & \text{for } s < 0 \\ 0.5 & \text{for } s = 0 \\ 1 & \text{for } s > 0 \end{cases}, \tag{3}$$

with $k_{\parallel}^{(\nu)}$ the modal loss parameter

$$k_{\parallel}^{(\nu)} = \frac{|V_{\parallel}|^2}{4W_{\text{tot}}} \quad , \quad V_{\parallel} = \int E_z^{(\nu)}(z) e^{jz\omega^{(\nu)}/c_0} dz, \tag{4}$$

$E_z^{(\nu)}(z)$ the longitudinal field on axis of mode ν, W_{tot} the total stored energy of mode ν, $p^{(\nu)} = -\omega^{(\nu)}/2Q^{(\nu)} + j\omega^{(\nu)}$ the complex eigenfrequency which is defined by the resonance frequency $\omega^{(\nu)}$ and the quality factor $Q^{(\nu)}$. Eq. (3) is valid for point like bunches. The wake of bunches with finite length σ is obtained by the convolution of the bunch shape and Eq. (3). For very short bunches ($\sigma\omega^{(\nu)}/c_0 << 1$) the convolution can be neglected, so that the energy loss of "bunch ς" is $W_{(\text{bunch}\,\varsigma)}^{(\text{modes})} = q^2 \sum_{(\text{bunches}\,\xi)} w_{\parallel}(s_{\varsigma\xi})$, with $s_{\varsigma\xi}$ the longitudinal distance between bunches ς and ξ. For constant bunch distance $s = T_{\text{bunch}}c_0$ and pulsed operation (T_{pulse}, f_{rep}) the power loss is:

$$P^{(\text{modes})} = f_{\text{rep}} q^2 \sum_{n=0}^{T_{\text{pulse}}/T_{\text{bunch}}} \sum_{m=0}^{n} w_{\parallel}(mT_{\text{bunch}}c_0)$$

or

$$P^{(\text{modes})} = f_{\text{rep}} q^2 \,\text{Re}\left\{\sum_{\nu} k_{\parallel}^{(\nu)} h\left(\exp\left(p^{(\nu)} T_{\text{bunch}}\right), T_{\text{pulse}} / T_{\text{bunch}}\right)\right\} \tag{5}$$

with $h(z,N) = (N+1)\frac{1+z}{1-z} - 2\frac{z - z^{N+2}}{(1-z)^2}$.

The power loss by one mode $P^{(\text{mode}\,\nu)}$ is maximal if the resonant frequency is a multiple of the bunch repetition frequency:

$$P^{(\text{mode}\,\nu)} = f_{\text{rep}} q^2 k_{\parallel}^{(\nu)} h\left(\exp(-T_{\text{bunch}} / \tau^{(\nu)}), T_{\text{pulse}} / T_{\text{bunch}}\right) \tag{6}$$

with $\tau^{(\nu)} = 2Q^{(\nu)} / \omega^{(\nu)}$. For long bunch trains and weak losses Eq. (6) simplifies to

$$P^{(\text{mode}\,\nu)} = f_{\text{rep}} T_{\text{pulse}} \left(\frac{q}{T_{\text{bunch}}}\right)^2 2R_s^{(\nu)}, \tag{7}$$

with the shunt impedance $R_s^{(\nu)} = 2k_{\parallel}^{(\nu)} Q^{(\nu)} / \omega^{(\nu)}$. Eq. (6) is used in sections 2.1.5 and 2.1.6 to estimate the peak losses per mode.

2.1.3. Modal Kick Parameters

The contribution of resonant modes to the transverse wake function is

$$w_{\perp}(s) = \text{Im}\left\{\sum_{\nu} 2k_{\perp}^{(\nu)} \exp\left(\frac{p^{(\nu)}}{c_0} s\right)\right\} \cdot \begin{cases} 0 & \text{for } s < 0 \\ 0.5 & \text{for } s = 0 \\ 1 & \text{for s} > 0 \end{cases}, \tag{8}$$

with $k_{\perp}^{(\nu)}$ the modal kick parameter

$$k_{\perp}^{(\nu)} = j\frac{\overline{V_{\parallel}} V_{\perp}}{4W_{\text{tot}}}\ ,\ V_{\perp} = \int \left(\mathbf{E}^{(\nu)}(z) + c_0 \mathbf{e}_z \times \mathbf{B}^{(\nu)}(z)\right) \cdot \mathbf{e}_{\perp} e^{jz\omega^{(\nu)}/c_0} dz\,. \tag{9}$$

$\mathbf{E}^{(\nu)}(z)$ and $\mathbf{B}^{(\nu)}(z)$ are the electrical field and magnetic flux density on axis of mode ν, $V_{\parallel}$ and W_{tot} are defined in Eq. 4 and $\mathbf{e}_{\perp}$ is the transverse unity vector perpendicular to the symmetries of the structure.

The kick parameters of the investigated setups should be not larger than the strongest kick parameters of the TESLA 9-cell cavities for an typical alignment error δ. The normalized longitudinal loss

parameter $k'_{\parallel} = k_{\parallel}(\delta)/\delta^2$ and the kick parameter $k_{\perp} = k_{\parallel} \cdot \delta \cdot \omega / c_0$ of the strongest dipole modes in the TESLA 9-cell cavity are listed in the following table for an offset δ=0.5mm,

f/GHz	$k'_{\parallel} = k_{\parallel}/\delta^2$ in V/(Cm²)	$k_{\perp} = k'_{\parallel} \cdot \delta \cdot c_0/\omega$ in V/C for δ = 0.5mm
1.71370	0.302E15	0.420E10
1.73828	0.423E15	0.581E10
1.86473	0.192E15	0.246E10
1.87265	0.256E15	0.326E10

2.1.4. Operational Conditions

The calculations of single bunch losses and resonant losses assume a repetition rate f_{rep} of 5Hz and a rf pulse length at flat top T_{pulse} of 0.95ms. Two types of operational modes are foreseen for the LINAC:

	collider operation	FEL operation
bunch length	400 μm	25 μm
bunch charge (current)	3.2 nC (9.5 mA)	1 nC (12 mA)
number of bunches (per pulse)	2820	11315

The resonant losses are calculated for the conductivity $\kappa = 2 \cdot 10^6 / \Omega m$ of steel at 2K.

2.1.5. Manual Valve Geometry 1

In the first version of a simplified valve the rf-shield is replaced by a fixed tube of the same diameter (78 mm) as the neighboring beam tubes. Fig. 1 shows a simplified sketch of this valve from the outside. In Fig. 2 cuts in the beam direction and in the vertical plane are shown. Once inserted into the beam position there will be a small gap between the tube and the beam pipes. In the following transient and resonant losses for gap sizes of 0.5 mm and 1.0 mm are calculated.

a) 0.5 mm gap

transient losses (Eq. (1)**)**

	collider operation σ = 400 μm	FEL operation σ = 25 μm
loss parameter V/C (MAFIA)	1.11E+11	5.91E+11
P_peak W	6.8	14.3
P_averaged mW	32	68

resonant losses **(**Eq. (6)**)** and kick parameter

f/GHz	Q	k_{loss}/(V/C)	P_{linac}/mW	P_{fel}/mW	k_t/(V/C)
0.183	252.	0.574E+08	0.023	0.034	0.133E+08
0.468	396.	**0.125E+11**	3.252	4.572	0.968E+09
0.663	112.	0.138E+09	0.020	0.012	0.356E+09
0.848	136.	0.162E+10	0.234	0.135	0.398E+10
0.972	585.	0.466E+09	0.095	0.122	0.158E+09
1.226	97.	0.436E+08	0.006	0.003	0.504E+09

1.251	103.	0.500E+09	0.072	0.031	0.277E+10
1.297	350.	0.127E+08	0.002	0.002	0.627E+08
1.449	796.	0.347E+08	0.007	0.008	0.206E+09
1.450	705.	0.137E+09	0.025	0.029	0.462E+08
1.595	599.	0.177E+08	0.003	0.003	0.520E+08
1.704	607.	0.321E+08	0.005	0.005	0.856E+08
1.974	220.	0.589E+08	0.009	0.004	0.123E+09
2.041	165.	0.602E+08	0.009	0.004	0.544E+08
2.128	262.	0.341E+09	0.049	0.024	0.129E+09
2.176	970.	0.237E+07	0.000	0.000	0.161E+08
lowest dipole cutoff frequency 2.25260 GHz					
2.261	130.	0.353E+08	0.005	0.002	0.330E+08
2.304	183.	0.337E+08	0.005	0.002	0.380E+08
2.401	514.	0.363E+06	0.000	0.000	0.276E+07
2.424	679.	0.453E+07	0.001	0.001	0.215E+07
2.484	boundary mode				
2.638	855.	0.250E+07	0.000	0.000	0.483E+07
2.688	678.	0.109E+08	0.002	0.001	0.106E+08
2.782	959.	0.304E+07	0.000	0.000	0.117E+07
2.815	1095.	0.161E+09	0.027	0.028	0.147E+08
lowest monopole cutoff frequency 2.94219GHz					
			Σ=3.851	Σ=5.022	

The electrical field distribution for mode 2 with the strongest longitudinal coupling is shown in Fig. 4.

b) 1.0 mm gap

transient losses (Eq. (1))

	collider operation $\sigma = 400\,\mu m$	**FEL operation** $\sigma = 25\,\mu m$
loss parameter V/C (MAFIA)	1.75E+11	8.66E+11
P_peak W	14.4	23.0
P_averaged mW	69	109

resonant losses (Eq. (6)) and kick parameter

f/GHz	**Q**	**k_{loss}/(V/C)**	**P_{linac}/mW**	**P_{fel}/mW**	**k_t/(V/C)**
0.219	310.	0.115E+09	0.046	0.070	0.308E+08
0.590	483.	**0.181E+11**	4.587	6.404	0.350E+09
0.659	191.	0.240E+09	0.036	0.032	0.665E+09
0.892	244.	0.538E+10	0.811	0.680	**0.100E+11**
1.034	667.	0.137E+10	0.293	0.385	0.843E+08
1.288	371.	0.201E+09	0.030	0.027	0.750E+09
1.313	240.	0.119E+08	0.002	0.001	0.276E+09
1.341	279.	0.184E+10	0.268	0.185	0.526E+10
1.460	725.	0.521E+09	0.096	0.114	0.800E+08
1.481	631.	0.529E+07	0.001	0.001	0.185E+09
1.604	590.	0.966E+08	0.016	0.016	0.223E+09
1.712	758.	0.122E+09	0.021	0.024	0.327E+09
1.998	354.	0.985E+08	0.014	0.009	0.293E+09
2.067	311.	0.231E+09	0.033	0.019	0.167E+09
2.159	534.	0.147E+10	0.219	0.171	0.570E+09
2.197	1400.	0.860E+07	0.002	0.002	0.558E+08
lowest dipole cutoff frequency 2.25260 GHz					
2.353	507.	0.398E+08	0.006	0.004	0.407E+08
2.369	boundary mode				
2.412	869.	0.116E+08	0.002	0.002	0.254E+08
2.467	394.	0.136E+08	0.002	0.001	0.409E+08
2.485	boundary mode				
2.640	858.	0.207E+08	0.003	0.003	0.240E+08
2.690	691.	0.448E+08	0.007	0.005	0.476E+08
2.780	1019.	0.159E+08	0.003	0.003	0.957E+07

2.814	1266.	0.378E+09	0.066	0.075	0.511E+08
2.941	635.	0.711E+10	1.043	0.739	0.328E+08
lowest monopole cutoff frequency 2.94219GHz					
			Σ=7.607	Σ=8.972	

2.1.6. Manual Valve Geometry 2

In the second version of a simplified valve the rf-shield is completely left out. Therefore the valve body could be reduced substantially in depth as shown in the cuts in the beam direction and in the vertical plane in Fig. 3. The transient and resonant losses are summarized in the following tables. The electrical field distribution for mode 5 with the strongest longitudinal coupling can be seen in Fig.5.

transient losses (Eq. (1))

	collider operation $\sigma = 400\,\mu m$	**FEL operation** $\sigma = 25\,\mu m$
loss parameter V/C	1.45E+12 (MAFIA)	6.3E+12 (diffraction)
P_peak W	44.0	76.2
P_averaged mW	209	362

resonant losses (Eq. (6)) and kick parameter

f/GHz	**Q**	**k_{loss}/(V/C)**	**P_{linac}/mW**	**P_{fel}/mW**	**k_t/(V/C)**
0.260	551.	0.864E+07	0.005	0.008	0.430E+08
0.672	623.	0.194E+10	0.543	0.777	0.319E+10
0.895	740.	0.523E+09	0.134	0.187	0.256E+09
1.262	705.	0.528E+08	0.010	0.013	0.129E+09
1.416	1313.	**0.174E+12**	48.634	69.573	0.497E+10
1.496	662.	0.895E+09	0.155	0.175	0.137E+10
1.689	610.	0.467E+09	0.075	0.076	0.420E+09
1.713	731.	0.149E+11	2.549	2.818	**0.311E+11**
1.864	722.	0.223E+10	0.367	0.385	0.207E+10
1.955	825.	0.348E+10	0.592	0.650	**0.142E+11**
2.113	1459.	0.918E+09	0.206	0.275	0.416E+09
lowest dipole cutoff frequency 2.25260 GHz					
2.265	951.	0.376E+09	0.064	0.070	0.235E+09
2.328	boundary mode				
2.478	862.	0.267E+10	0.424	0.417	0.182E+10
2.659	1998.	0.164E+08	0.004	0.005	0.894E+08
2.694	1282.	0.509E+08	0.009	0.011	0.265E+08
2.823	1291.	0.441E+10	0.777	0.889	0.257E+10
2.860	1278.	0.445E+10	0.776	0.878	0.545E+09
lowest monopole cutoff frequency 2.94219GHz					
			Σ=55.32	Σ=77.21	

2.2. Fields Induced by the Cavities

High frequency wake field components (up to several THz) which are caused in the cavities are a strong contribution to the electrical losses in the valve walls. Although it is almost impossible to calculate the propagation and multiple scattering of these fields in one ore more modules, the total excitation can be computed from the short range wake. From the analytical approximation [3] of the point charge wake potential the total power loss per module above a given frequency is plotted in Fig.

6. For collider operation (500 GeV) the total losses in one module (12 nine cell cavities) are 23.3 W, for FEL operation they are 14.2W. To absorb these losses a cylinder of highly absorbing material is foreseen in the interconnection between modules [4,5]. The absorber operates at a temperature of approximately 70K where the refrigerator efficiency is much better than at 2K or 4K. The geometry of the absorber is sketched in Fig. 7, the estimated material properties are shown in Fig. 8. The material parameters are taken from from [6] for AlN (glassy) and are extrapolated for high frequencies with $\varepsilon_r'' = -\mathrm{Im}(\varepsilon_r) \propto 1/\omega$. As the manual valves on both sides of the interconnection are coupled to the 2K level, the losses in the valve walls contribute significantly to the required cryogenic power. In the following the absorber efficiency

$$\eta = \frac{P_{\text{absorber}}}{P_{\text{tot}}} \approx \frac{P_{\text{absorber}}}{P_{\text{absorber}} + 2P_{\text{valve}}} \tag{10}$$

is estimated, with P_{tot} the total loss of beam power in one module, P_{absorber} the dissipated power in the absorber and P_{valve} the power loss per valve. This estimation is based on the assumption that the cavity wake field can be characterized by a photon gas [5]. The density of the photon gas is described by $D_{r,e}(\vec{r},\vec{e})$, with $\vec{r}$ the 3d spatial location and $\vec{e}$ the unity vector into the direction of propagation. In structures with symmetry of revolution $D_{r,e}(\vec{r},\vec{e})$ can be simplified for monopole fields to $D_{rz,\varphi}(\rho,z,\varphi)$ with $\vec{r} = \rho\vec{e}_r + z\vec{e}_z$ and $\cos\varphi = \vec{e}\cdot\vec{e}_z$. To obtain a one dimensional model for the density in a **perfect conducting beam pipe** ν from $z_{\nu,\mathrm{a}}$ to $z_{\nu,\mathrm{b}}$, we assume that $D_{\rho z,\varphi}(\rho,z,\varphi)$ is independent on z and ρ and proportional to $\cos\varphi$ [5]. Therefore $D_{\rho z,\varphi}(\rho,z,\varphi)$ can be written as

$$D_{\rho z,\varphi}(\rho, z_{\nu,\mathrm{a}} \le z < z_{\nu,\mathrm{b}}, \varphi) = \begin{cases} a_\nu \cos\varphi & \text{if } \cos\varphi > 0 \\ b_\nu |\cos\varphi| & \text{otherwise} \end{cases}, \tag{11}$$

with a_ν proportional to the number of photons per unit length in forward direction and b_ν proportional to photons in backward direction. A complex geometry composed by photon scattering, photon generating and photon absorbing objects as cavities, valves and absorbers that are connected by beam pipes can be described by linear two-port equations as it is shown in Fig. 9. The matrix equation for each of these objects has the form

$$\begin{pmatrix} b_\nu \\ a_{\nu+1} \end{pmatrix} = \underbrace{\begin{pmatrix} s_{11} & s_{12} \\ s_{21} & s_{22} \end{pmatrix}}_{S} \begin{pmatrix} a_\nu \\ b_{\nu+1} \end{pmatrix} + \underbrace{\begin{pmatrix} g_1 \\ g_2 \end{pmatrix}}_{G}. \tag{12}$$

The parameters on the left hand side $b_\nu, a_{\nu+1}$ describe photons which propagate out of the component, the other two parameters $a_\nu, b_{\nu+1}$ represent photons propagating into the component. S is the

scattering matrix and G the generator vector. In the following the linear equation (12) is worked out for the valve, absorber and module.

a) The **absorber** is sketched in Fig. 7. It is symmetric, reflection free and no photons are generated in the inside. Therefore it is characterized by

$$S_{\text{absorber}} = \begin{pmatrix} 0 & \tilde{T} \\ \tilde{T} & 0 \end{pmatrix},\ G_{\text{absorber}} = \begin{pmatrix} 0 \\ 0 \end{pmatrix}, \tag{13}$$

with $\tilde{T}$ the transmission probability. The frequency dependent transmission probability $\tilde{T}$ is obtained by calculating the weighted mean value $\left\langle \tilde{t}(\rho,\varphi)\, p(\rho,\varphi) \right\rangle$ of the transmission probability $\tilde{t}(\rho,\varphi)$ of photons, which start from the left boundary with the initial conditions $\rho, \varphi, \cos\varphi > 0$. As we assumed that the photon probability is independent on the offset and proportional to $\cos\varphi$ the weighting function is $p(\rho,\varphi) = \cos\varphi \big/ \left\langle \cos\varphi \right\rangle$. The function $\tilde{t}(\rho,\varphi)$ is calculated by geometrical optics. The reflection probability at the surface of the absorbing material is based on a plane wave model. Fig. 8b shows the transmission probability $\tilde{T}$ as function of the frequency.

b) The **manual valve** is longitudinally symmetric and free of photon generation:

$$S_{\text{valve}} = \begin{pmatrix} R & T \\ T & R \end{pmatrix},\ G_{\text{valve}} = \begin{pmatrix} 0 \\ 0 \end{pmatrix}, \tag{14}$$

with R and T the reflection and transmission probabilities. The simplified model for the calculation of geometry 1 is sketched in Fig. 10. This model replaces the two gaps by one gap of twice the width and assumes that all photons which hit the gap are completely absorbed due to a large number of multiple reflections in the absorber box. According to this assumption the reflection R vanishes and $T = \left\langle t(\rho,\varphi)\, p(\rho,\varphi) \right\rangle$ is frequency independent. A simplified configuration for the estimation of the second valve geometry is sketched in Fig. 11: the valve housing is replaced by a pillbox cavity with the same inner surface. The weighted mean values of the reflection and transmission coefficients are calculated in tow steps: $t(\varphi) = \left\langle t(\rho,\varphi) \right\rangle_\rho$, $r(\varphi) = \left\langle r(\rho,\varphi) \right\rangle_\rho$ and $T = \left\langle t(\varphi)\, p_\varphi(\varphi) \right\rangle_\varphi$, $R = \left\langle r(\varphi)\, p_\varphi(\varphi) \right\rangle_\varphi$ with $\langle\ \rangle_\rho$ the averaging operator in ρ direction, $\langle\ \rangle_\varphi$ the averaging operator in φ direction and $p_\varphi(\varphi) = \cos\varphi \big/ \left\langle \cos\varphi \right\rangle_\varphi$. The reflection probability at the steel surface of the housing is based on a plane wave model. Although the photons are scattered in a complicated manner into forward and backward direction (see Fig. 12a), the escape probability $t(\varphi) + r(\varphi)$ is almost a smooth function of the angle φ (see Fig. 12b). The properties T, R, $T + R$ are plotted in Fig. 13.

c) The **module** is longitudinally symmetric and the losses are negligible compared to that of the absorber and the manual valves. The scattering matrix and the generation vector are:

$$S_{\text{module}} = \begin{pmatrix} 1-t & t \\ t & 1-t \end{pmatrix},\ G_{\text{module}} = \begin{pmatrix} g \\ g \end{pmatrix}, \tag{15}$$

with t, g the transmission and generation coefficients. Due to the symmetry given by the periodic boundary conditions (compare Fig. 9) the same number of photons $a_0 = b_1$ propagates from both ends into the structure and the same number of photons $b_0 = a_1$ leaves it on both sides. Therefore the resulting matrix equation is independent on the transmission coefficient t. The generation coefficient g is identical to the spectral power density $p(\omega)$, which is given by the negative derivative $-dP(\omega)/d\omega$ of the fractional power losses in Fig. 6.

The frequency dependent absorber efficiency η is defined as ratio $P_{absorber}/P_{tot}$ of the total photon power

$$P_{tot} = 2(a_1 - b_1) = 2\left(1 - R - \frac{T^2\tilde{T}}{1 - R\tilde{T}}\right)a_1 \tag{16}$$

and the power of the photons which are dissipated in the absorber

$$P_{absorber} = 2(a_2 - b_2) = 2\frac{T(1-\tilde{T})}{1 - R\tilde{T}}a_1 . \tag{17}$$

Therefore the efficiency is

$$\eta = \frac{T(1-\tilde{T})}{(1-R)(1-R\tilde{T}) - T^2\tilde{T}}, \tag{18}$$

and the induced power losses per valve are given by

$$P_{valve} = \frac{1}{2}\int_0^\infty p(\omega)(1-\eta(\omega))\,d\omega . \tag{19}$$

The absorber efficiencies of geometry 1 and 2 are plotted in Fig. 14, the power losses per valve are listed in the following table.

	Collider operation σ = 400 μm	**FEL operation** σ = 25 μm
geometry 1, 0.5 mm gap	0.503 W	0.288 W
geometry 2, 1.0 mm gap	0.935 W	0.536 W
geometry 2	0.419 W	0.357 W

3. Results

The strongest source of losses in the manual valve are losses due to wake fields induced by the cavities. For the linac operation mode one expects for each valve losses of 500 mW for valve geometry 1, 0.5 mm gap, 940 mW for geometry 1, 1.0 mm gap and 420 mW for geometry 2. Compared to this, losses due to fields induced by the valves themselve are small if a valve with simple rf-shield (geomety 1) is used. These losses can be split into transient and resonant losses and are strongest in the FEL operation mode. The transient losses are essentially not absorbed in the valve because the high frequent wake fields propagate through the structure. Assuming an absorber efficiency of 90% only 10% of these losses will be dissipated at 2 or 4 K . The resonant losses are about a factor 10 smaller than the transient ones and will be completely absorbed in the valve. The results are summarized in the following table.

	geometry 1 0.5 mm gap	geometry 1 1.0 mm gap	geometry 2
losses due to wake fields induced by the cavities (linac operation)	500 mW	940 mW	420 mW
transient losses (FEL operation)	68 mW	109 mW	360 mW
resonant losses (FEL operation)	5 mW	9 mW	77 mW
ratio of the strongest transverse kick by the valve and by the cavity (0.5 mm offset)	0.7	1.7	5.4

Due to the transverse asymmetry of the valve geometry an asymmetric field and thus a transverse kick is generated. The ratio of the strongest kick per mode by the valve and the cavity for an offset of 0.5 mm are also summarized in the above table. The kicks for the valve of geometry 1 are comparable to the one of the cavity, for the geometry 2 the kick is a factor 5.4 stronger.

4. Conclusion

For the TESLA modul losses by wake fields in the manual valve have been studied in detail. Two valve geometries, one with a simple rf-shield (geometry 1) and one without rf-shield (geometry 2) have been investigated. Three types of losses can be distinguished: transient and resonant losses due to wake fields induced by the valves themselves and losses due to wakes induced in the cavities. The calculations have been done for two different operation modes – linac operation and FEL operation. In addition the transverse kick has been calculated.

The losses of the valve with geometry 1, 0.5 mm gap are acceptable, the kick is smaller than the one from the cavity. Increasing the gap to 1.0 mm increases the losses to an unacceptable level, while the kick would be still acceptable. The valve of geometry 2 has an unacceptable high kick, the losses are still reasonable.

Following these calculations it becomes clear that the manual valve must have an rf-shield. For further studies of the TESLA module a valve with simple rf-shield and small gap (0.5 mm) is assumed.

References

[1] The MAFIA Collaboration, CST GmbH, Buedinger Str. 2a, D-64289 Darmstadt, Germany.

[2] B.Zotter, S.Keifets: Impedances and Wakes in High-Energy Particle Accelerators. World Scientific 1998.

[3] R.Brinkmann, M.Dohlus, D.Trines, A.Novokhatki, M.Timm, T.Weiland, P.Hülsmann, C.T.Rieck, K.Scharnberg, P.Schmüser: Terahertz Wakefields in the Superconducting Cavities of the TESLA-FEL Linac, TESLA 2000-07, March 2000.

[4] A.Jöstingmeier, M.Dohlus, M.Wendt, C.Cramer: Theoretical and Practical Investigations Concerning the Design of a HOM Broadband Absorber for TESLA, TESLA 2000-10, July 2000.

[5] A.Jöstingmeier, M.Dohlus: Photon Diffusion Model for TTF-2, TESLA 2000-11, July 2000.

[6] B.Mikijeli, E.Campisi: Development of an artificial dielectric ceramic for use at CEBAF, Proceedings of the Workshop on Microwave-Absorbing Materials for Accelerators, 1993 Newport News, Virginia.

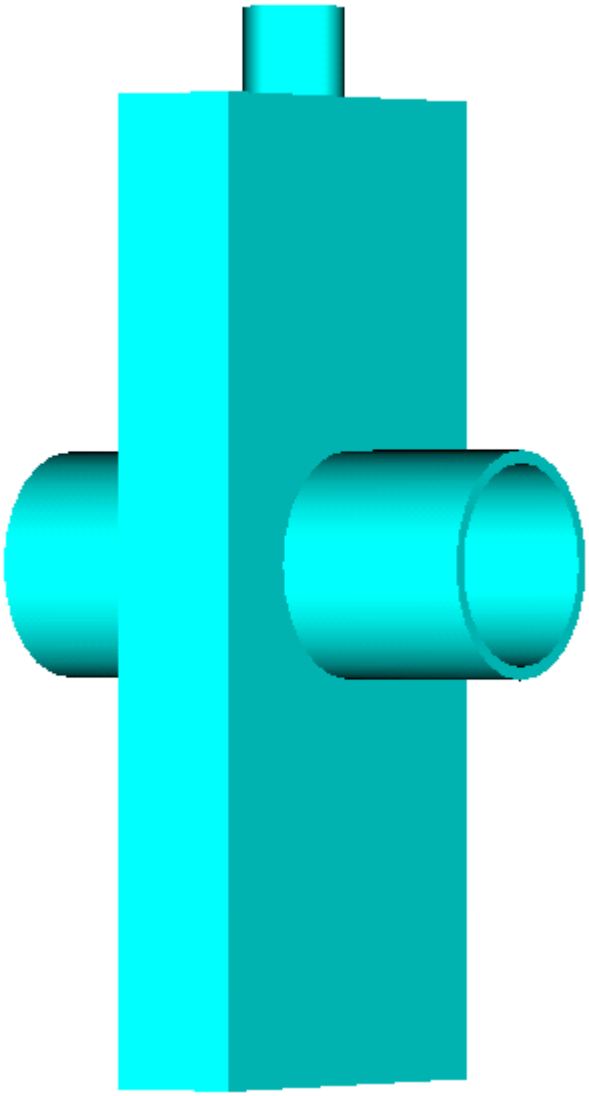

Fig. 1: Schematic sketch of the simplified valve of geometry 1 from the outside.

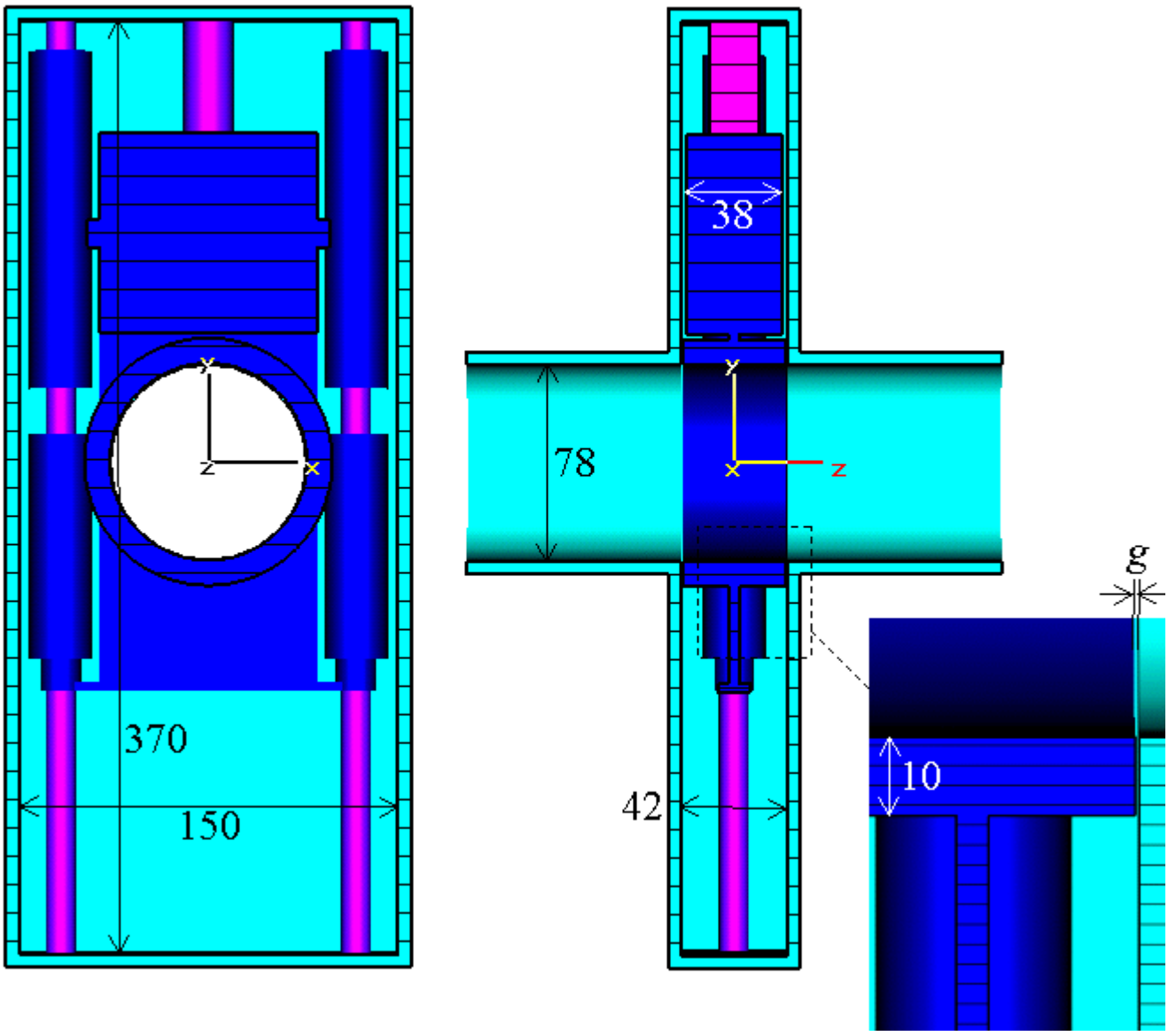

Fig. 2: Cuts in the beam direction and in the vertical plane for a simplified valve of geometry 1. An enlarged view of the area of the gap g between the tube and the neighboring beam pipes is shown as well.

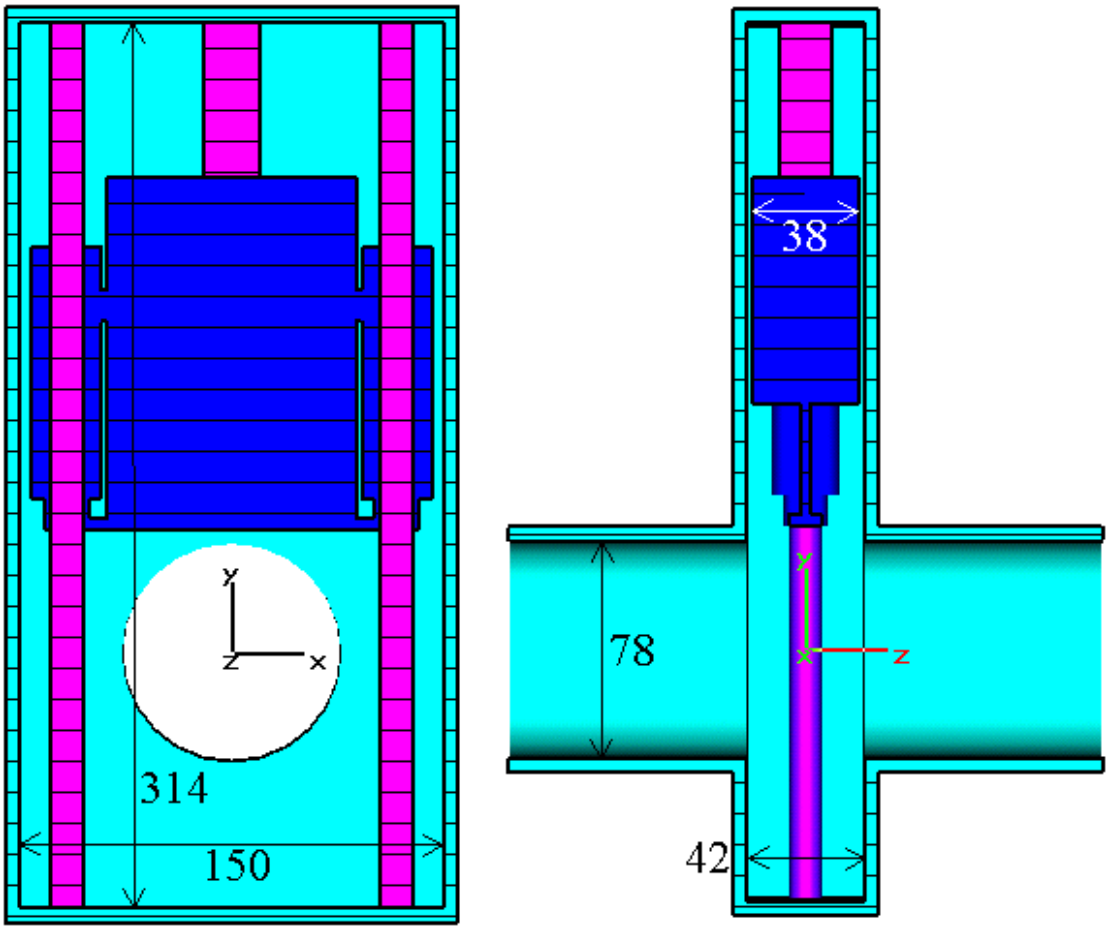

Fig. 3: Cuts in the beam direction and in the vertical plane for a simplified valve of geometry 2.

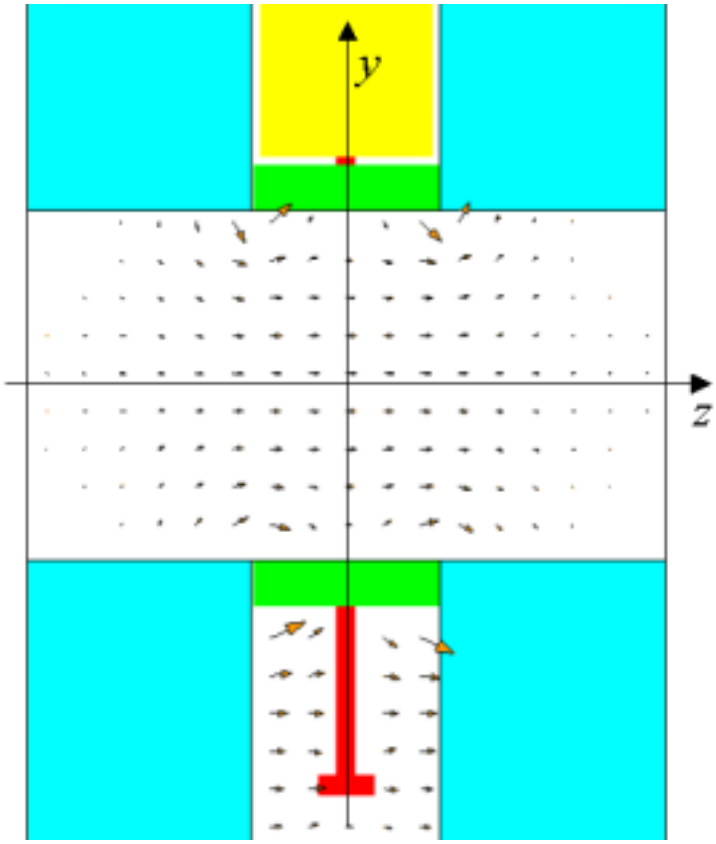

Fig. 4: Field distribution in the valve of geometry 1, 0.5mm gap for mode 2.

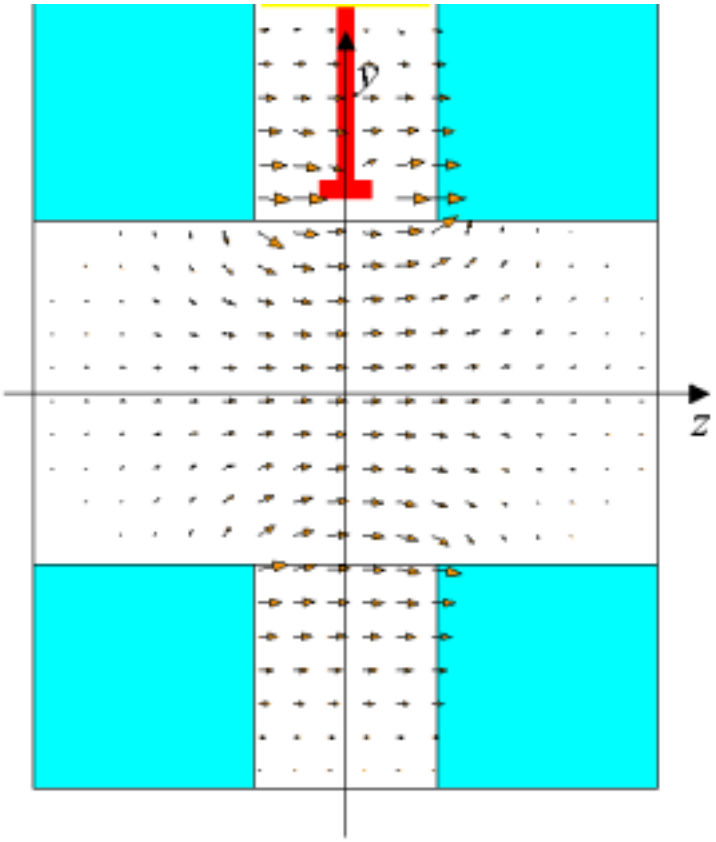

Fig. 5: Field distribution in the valve of geometry 2 for mode 5.

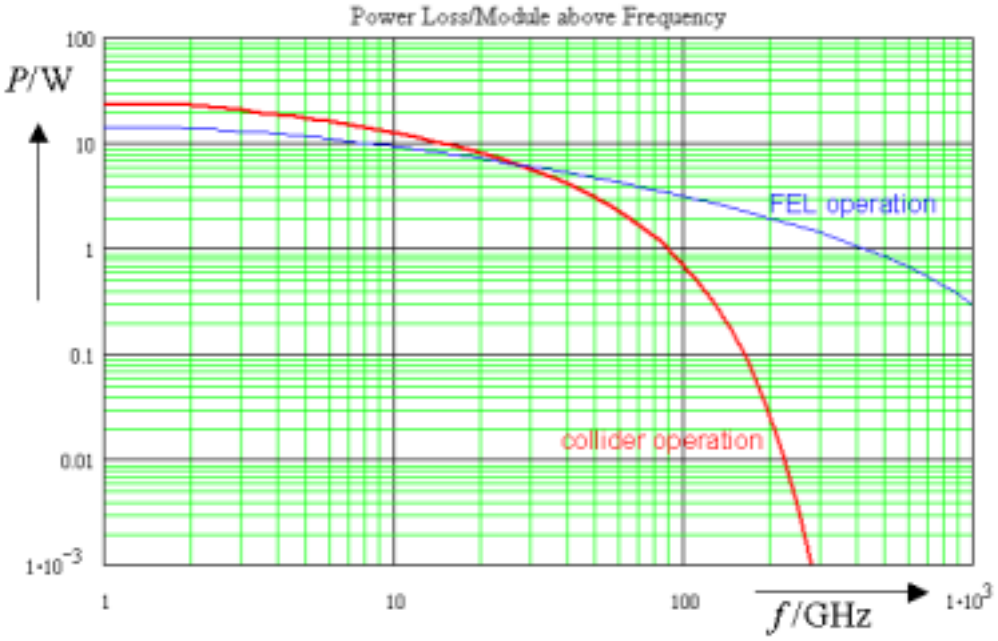

Fig. 6: Fractional part of the power losses of one cryo-module (with 12 9-cell cavities) above a lower frequency boundary for collider and FEL operation.

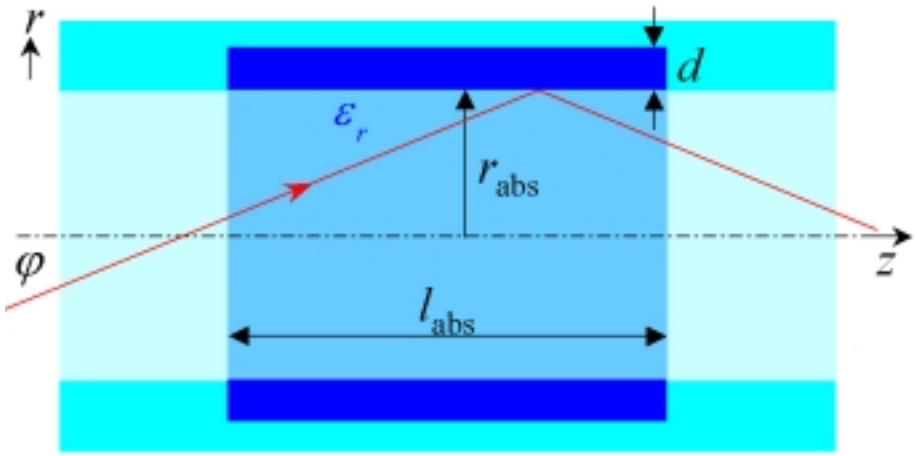

Fig. 7: Geometry of Absorber, l_{abs} = 100 mm, d = 10 mm.

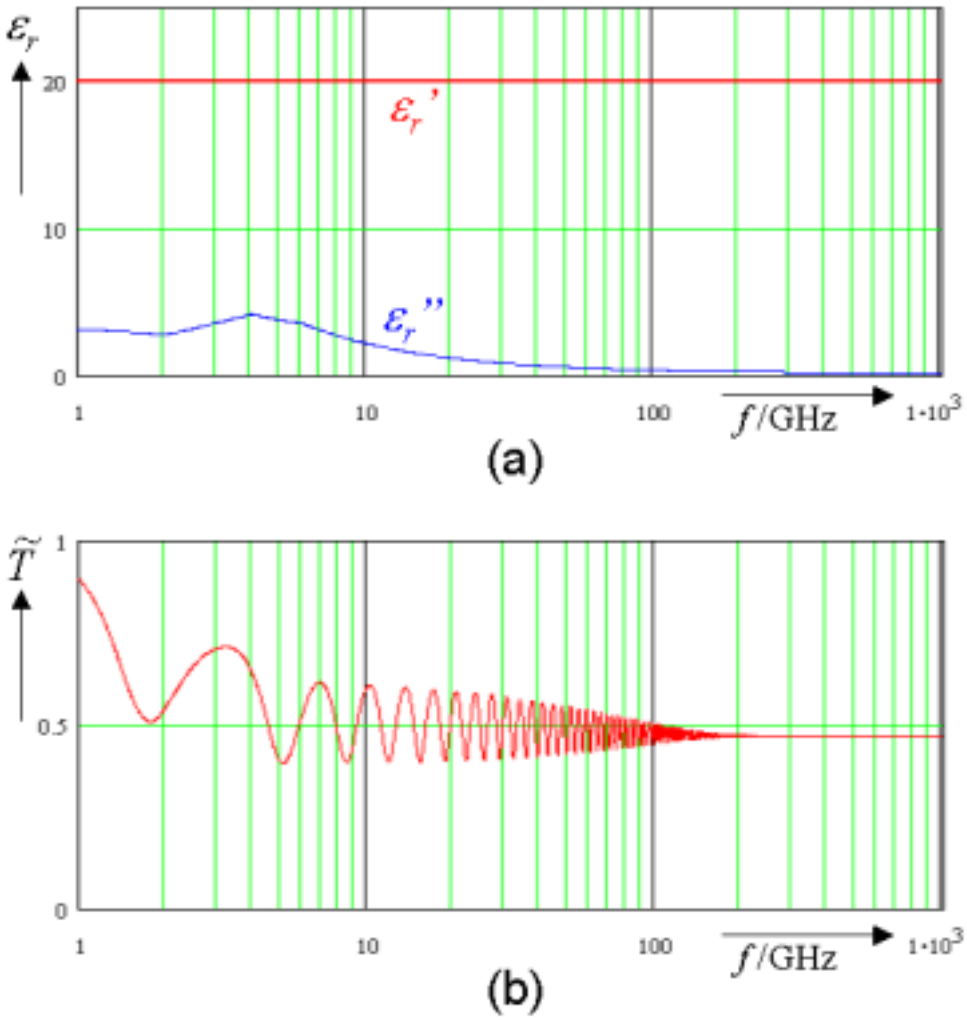

Fig. 8: (a) Complex permittivity $\varepsilon_r = \varepsilon_r' - j\varepsilon_r''$ of the absorber material, (b) averaged transmission probability.

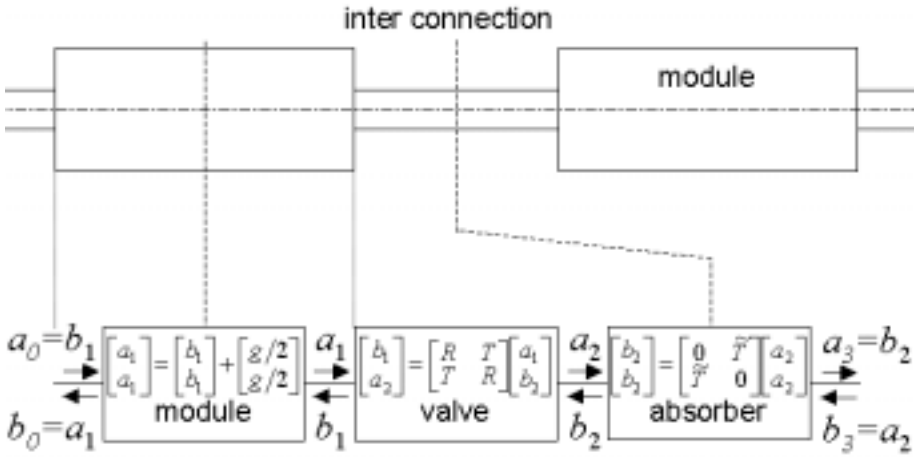

Fig. 9: Scattering matrix model.

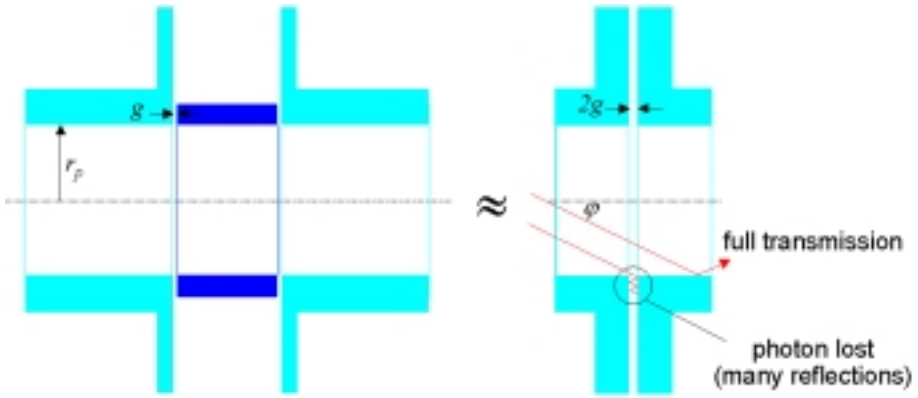

Fig. 10: Simplified model for the transmission probability in manual valve “geometry 1”.

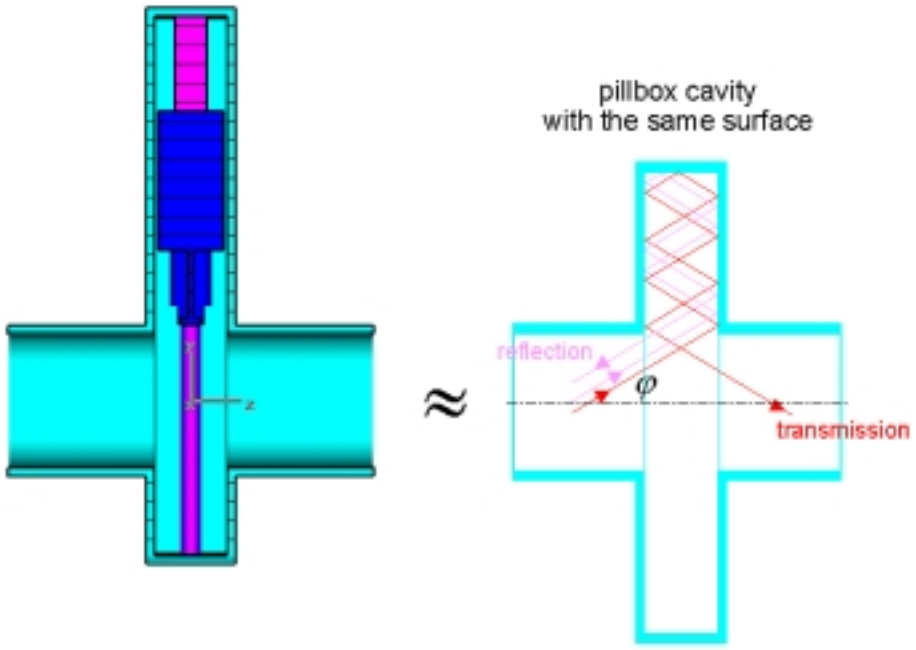

Fig. 11: Simplified model for the reflection and transmission probability in manual valve “geometry 2”.

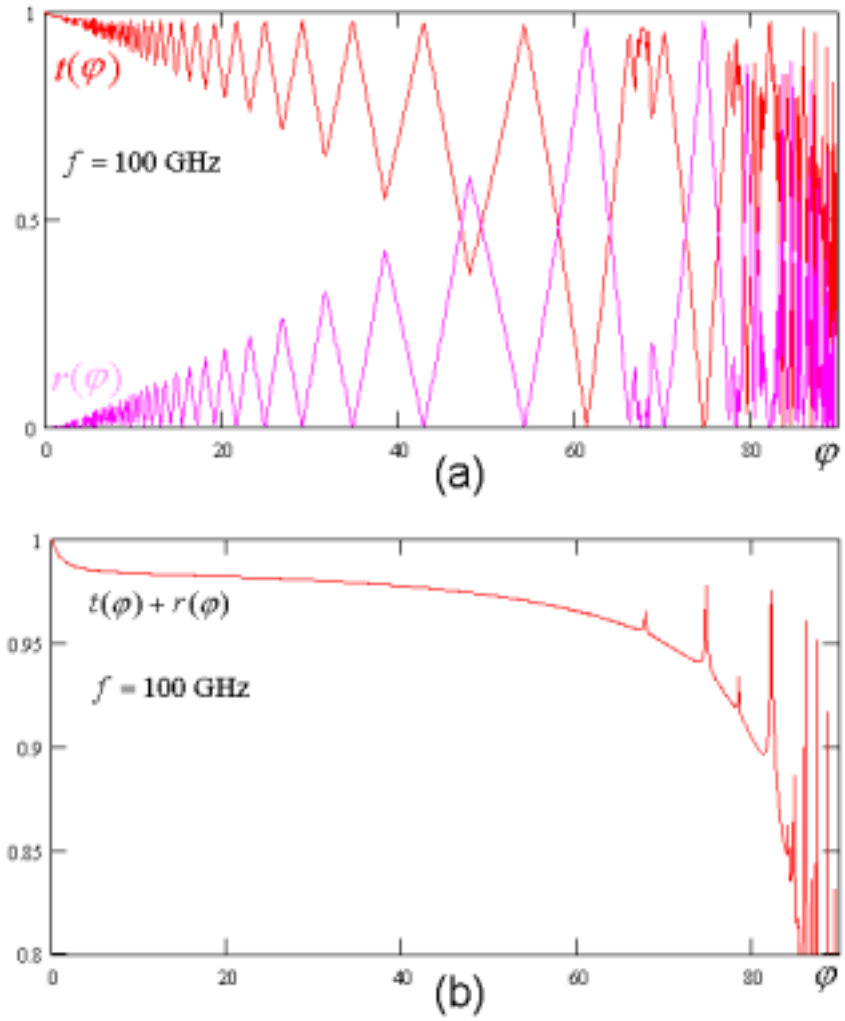

Fig. 12: (a) Reflection and transmission probability $r(\varphi)$, $t(\varphi)$ for the simplified model ("geometry 2") at 100 GHz, (b) Escape probability $r(\varphi)+t(\varphi)$ at 100 GHz.

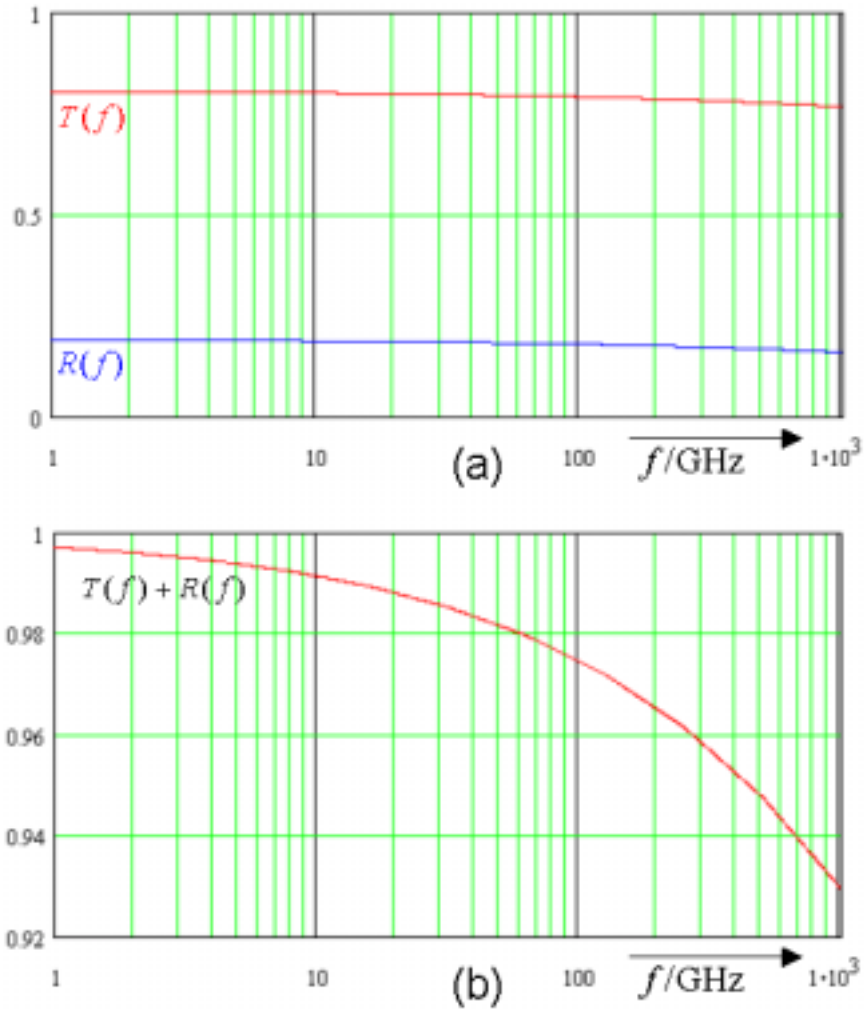

Fig. 13: (a) Averaged reflection and transmission probability $R(\varphi)$, $T(\varphi)$ for the simplified model ("geometry 2"), (b) Averaged escape probability $R(\varphi)+T(\varphi)$.

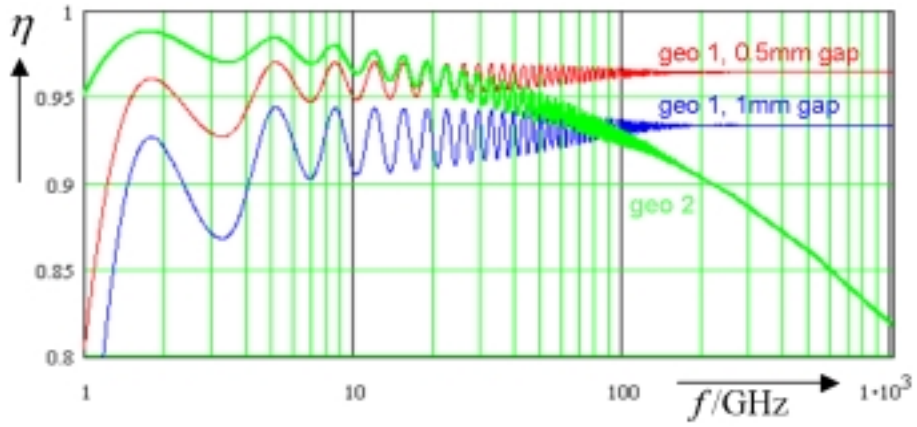

Fig. 14: Absorber efficiencies for the two types of valve geometries.